Optica Applicata, Vol. XXVII, No. 2, 1997

Production of diffraction kinoform elements using laser printer

M. KACZURBA, J. NOWAK

Institute of Physics, Technical University of Wrocław, Wybrzeże Wyspiańskiego 27, 50–370 Wrocław, Poland.

When constructing a hybrid lens as a refractive lens (90–95% focal power) connected with the diffractive one (5–10% focal power), the diffractive part is assumed to play part of the correcting filter. Such a filter is manufactured as kinoform (2π phase depth) and used for correcting lens aberrations. Since it includes no structures of high spatial frequencies, the due manufacturing process in laboratory conditions is easy and cheap. The process consists of two steps. Step 1 – a binary model of the filter is produced using a 600 dpi laser printer, step 2 – during the photoreduction process the binary model is converted into continuous filter applying the bleaching process to holographic silver halide material. A few methods of binarization (continuous to binary conversion) during the experiment and the computer simulation are analysed. Using Mach–Zehnder interferometer some saw-tooth filters are examined and their quality, efficiency, phase depth and spatial frequency are estimated. During experiment a good quality filter is obtained, but the phase depth is smaller than 2π. It changes with spatial frequency and strongly depends on both recording media and photochemical processing, and therefore some further investigations are needed. Because of promising results the next step to follow is to calculate and manufacture an aberration-correcting filter for the spherical glass lens and to investigate photopolymers as the recording media.

1. Introduction

In the contemporary optics the hybrid elements are of increasing use. The simplest hybrid element is a classic glass lens with a diffraction structure deposited on one of its sides. The problem of designing such a lens was considered in many papers, *e.g.*, [1], [2]. The dioptric power of the diffractive part of such a hybrid element is usually small ranging within 5–10% of the total power. Thus, it may be treated as a correcting filter.

Due to the necessity of achieving a great diffraction efficiency such a filter should be produced as a kinoform. There are a number of production technologies used nowadays [3]–[9], most of them being complicated because of the sizes and properties of the structure elements of order of λ. If, however, the kinoform correcting filter is not required to be of high spatial frequency structure, it can be produced in a relatively easy and not too expensive way.

The objective of this work was to provide a method of inexpensive filter production with the aid of 600 dpi laser printer. For this purpose, the methods of presenting continuous structures on binary devices [10]–[14] were adapted, the calculated filter matrices were printed and the filters of continuous structure

were produced using photoreduction technique. This process was next simulated on a computer, taking into account the phenomena influencing the quality of the elements obtained, and the results were compared with experimental ones.

2. Comparison of different methods

Nowadays, different methods of production of diffractive optical elements (DOE) are used (differing in the ways of production, labour consumption, complexity of the devives used) to manufacturing filters of different quality and different production costs. The kinoform filter, for example, the correcting aberrations, should produce a wavefront described sometimes by a complex function, and therefore the methods enabling a simple and immediate transfer of the data from the computer to the kinoform filter [7]–[9], [14], [15], become of practical importance. Worse methods of narrower applicability are those based on recording the interference or holographic image [6], since in this way only a limited number of simple structures can be written down, such as diffraction gratings or spherical lenses. Below, two technologically advanced methods are described which constitute a reference level to estimate the method of kinoform structure production (Subsect. 2.3) proposed in this paper.

2.1. Direct laser beam-writing method

The technology of direct laser beam-writing provides a kinoform diffraction element (KDE) of theoretical diffraction efficiency independent of the spatial frequency and amounting to 100% [7]. In practice, a loss of diffraction efficiency, with the increase of spatial frequency, is observed up to some cut-off frequency, which is due to different effects appearing during production of KDE with this method. Above all these are: diffraction at the microstructure of the material and discrete steering of the process. There exists a possibility of increasing the cut-off frequency by increasing the phase modulation depth of the kinoform up to the value 4π, 8π and higher multiples of 2π, but because of the complexity and required precision of the due aperture this method is expensive.

Theoretically, the direct laser-beam writing method is perfect, rendering it possible to produce an element of practically any profile and therefore it has been used as a reference method to define the quality and to measure the diffraction efficiency achieved by other methods. It has also been used for analysis of perturbances introduced by filter when changing its parameters.

In this work, the structure obtained by this method is considered to be continuous in contrast to the binary or quantized structures. This means that the element of continuous structure obtained by this method is free from any discontinuity regions outside those of phase shift 2π which stem from the definition of kinoform.

For the purpose of analysis, a one-dimensional model of optical wedge has been used, with its phase φ being described by a saw-tooth function

$$\varphi(x) = 2\pi(x - [x]) \tag{1}$$

where $[x]$ denotes the integer part of x.

The complex amplitude is given by the relation

$$A(x) = A_r \exp(i\varphi), \tag{2}$$

which for saw-tooth phase element of φ defined by (1) and $A_r(x) = 1$ gives

$$A(x) = \exp(2\pi i(x - [x])). \tag{3}$$

The kinoform of such an object is a saw-tooth diffraction grating (Fig. 1a) and the whole beam incident to such a filter will be diffracted into first order of diffraction (Fig. 1b).

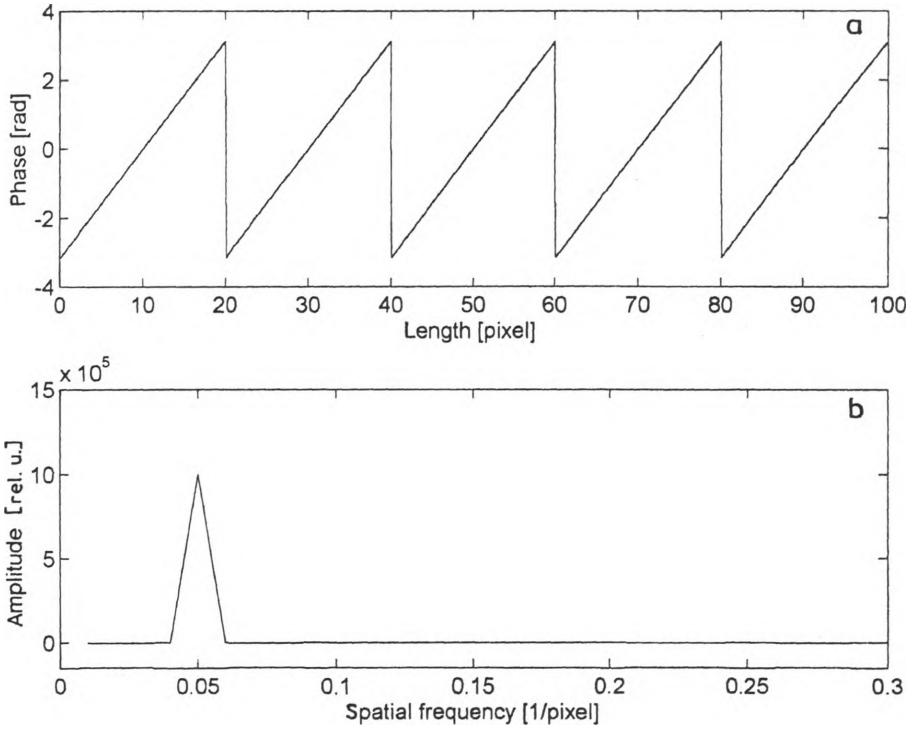

Fig 1. Fragment of the phase kinoform profile in the form of a saw-tooth phase diffraction grating (a). Intensity Fourier transform $F^2\{A(x)\}$ of this kinoform (b)

In order to determine the quality of the filters produced by using different methods their phase profiles were compared with that defined by (1) and the r.m.s deviation was calculated

$$D\varphi(x) = \sqrt{|\varphi_1(x)^2 - \varphi_2(x)^2|}. \tag{4}$$

The Fourier transforms of these filters were compared calculating the differences with respect to the squared modulus of the Fourier transform $I(v)$ (called further the intensity in the Fourier plane) of the complex amplitude function (3)

$$\Delta I(\nu_x) = I\{A_1(x)\} - I\{A_2(x)\}; \quad I(\nu) = F(\nu)F^*(\nu) \tag{5}$$

and the diffraction efficiency was calculated being understood as the ratio of intensity of the first order diffraction signal (3) to that of the corresponding incident light

$$\eta = \frac{I_2(\nu_1)}{I_1(\nu_1)} 100\%. \tag{6}$$

While analysing the filters both the examined and perfect profiles were drawn on the figures presenting the phase profiles and below the differences of these two profiles (4). In the figures representing Fourier transforms the intensity in the Fourier plane of the examined and ideal profile and the error of the intensity $\Delta I(\nu)$ in the Fourier plane (5) were presented in sequence from the upper to the lower part of the figure.

2.2. Mask-based electron beam lithography method

Multistep electron lithography provides elements of stepped structure (4)

$$\varphi(x) = \frac{2\pi}{2^N - 1}([2^N x] - 2^N[x]) \tag{7}$$

where N is the number of masks used in the process of producing the elements.

The efficiency of this method depends on the number of the applied masks N; for $N \geqslant 3$ the theoretical efficiency amounts to $\eta \geqslant 94\%$ [5], [6], [15]. It depends on the spatial frequency of the element and has a threshold value. In practice, the efficiency suffers from some lowering due to the errors of the mask positioning during the etching process, diffraction at the rim of the mask, and restrictions of the least size of the mask elements [16]. This method requires high accuracy of performance and mask positioning, at least, by an order of magnitude better than that for the kinoform itself while being labour consuming and expensive.

2.3. Half-tone kinoform filter

In this paper, a simple two-stage method of generating kinoform of continuous phase (Fig. 2) is presented. This method can be perfectly applied under the simple laboratory conditions being simultaneously an economic method of producing the optical diffraction elements for the purposes of experiment.

In the first stage the mathematical function describing the kinoform (Fig. 2a) is transformed into a binary form (Fig. 2b). In this form, the phase is encoded by randomly distributed black points on a white background (Fig. 2c) in such a way that density of the points in an arbitrary region is proportional to the average value of phase in this region. Next, this matrix is printed on a 600 dpi laser printer.

The second stage is the photoreduction of the matrix obtained in this way on the kinoform material (Fig. 2d). During this process the spread function is introduced in order to produce the element of continuous phase (Fig. 2e). The photoreduction occurs in the scattered white light using high resolution objective and the spread function is introduced by slightly defocusing the image.

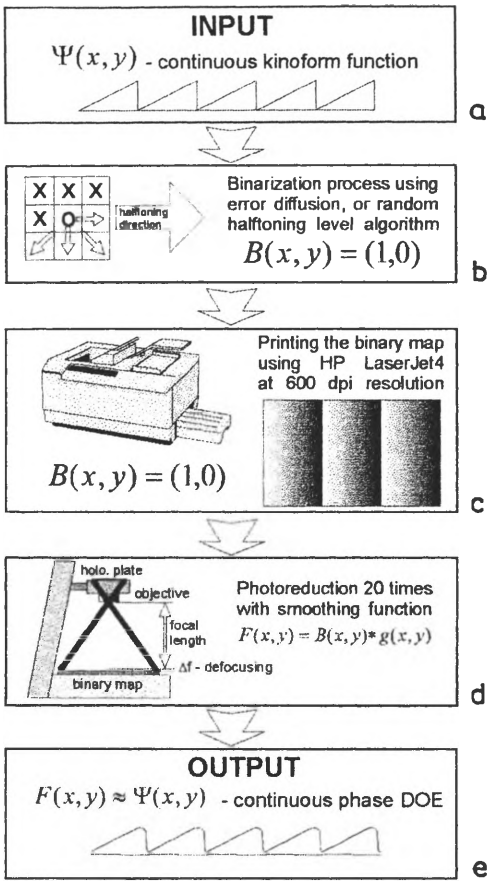

Fig. 2. Scheme of the proposed two-stage method of producing the half-tone kinoform filters (for details, see the text)

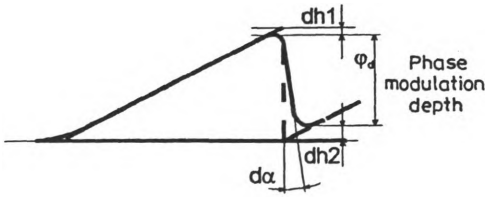

Fig. 3. Profile of the tooth obtained as a result of half-tone method of generating the kinoform filters

For the constant spread function of the kinoform produced by half-toning and convolving it with the spread function the limiting case can be determined being characterized by the greatest diffraction efficiency. It defines the theoretical diffraction efficiency of this method and is achieved by the infinitely dense sampling of the

function describing the kinoform, *i.e.*, the step of the half-toning process tends to zero. The profile of one tooth of the saw-tooth function (1) after ending this process differs from the initial profile (Fig. 3). These differences $dh1$, $dh2$ affecting the depth of phase modulation of the kinoform would be taken into account while designing the function in order to assure the phase fitting of the produced element. A fragment of the tooth of opposite slope $d\alpha$ influences the lowering of the efficiency of the filter produced in this way and cannot be diminished under the assumption of constant width of the spread function.

Similarly, as was the case for the mask-based electron beam lithography, an analysis of this process was performed, the differences between the profiles $D\varphi$ and the error of the intensity in the Fourier plane ΔI for ideal kinoforms and those obtained in the process as well as the diffraction efficiences were calculated for the two cases: the same spatial frequency of the kinoforms and different spread functions as well as different spatial frequencies of kinoforms and the same spread function.

As it should be expected, together with the diminishing of the spread function half-widths (more sharp imaging), a qualitatively better hologram is obtained; the kinoform quality increases also with diminishing of its spatial frequency. Obviously, for a proportionally changing spread function and the spatial frequency of the kinoform the diffraction efficiency does not suffer from change.

In accordance with the above results when both the sampling step and the spread function half-width tend to zero, we obtain an ideal kinoform described by (1) as a limiting case. However, in practice the real sampling step has finite dimension and the spread function must cover at least three or four sampling cells to justify its application.

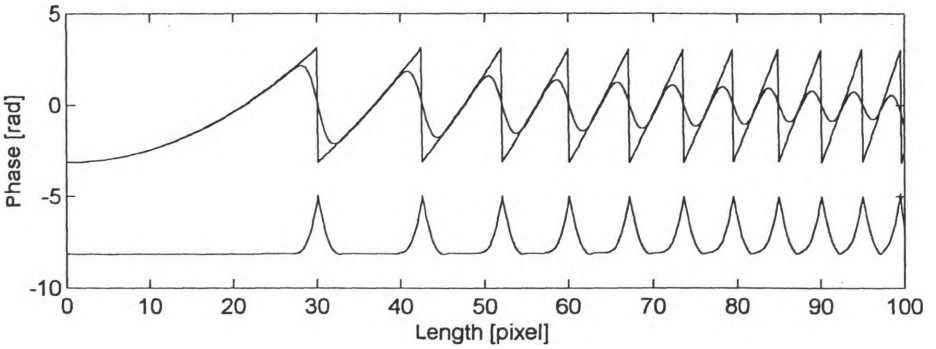

Fig. 4. Phase profile of the filter of changing spatial frequency. The drop of modulation depth with the increase of spatial frequency is visible

For some constant spread function together with the increase of the spatial frequency the modulation depth decreases down to certain limiting values, for which the elements of the structure influence each other to such a degree that they become indistinguishable (Fig. 4). For this case, the analysis was applied to the function of spatial frequency, the phase of which is described by the function

$$\varphi(x) = 2\pi(x^2 - [x]^2). \tag{8}$$

3. Description of the experimental method

The experiment was carried out in strict accordance with the scheme (Fig. 2) described in Subsec. 2.3. The influence of its particular stages on the final result as well as the intermediate results was examined. For this purpose, the saw-tooth function (1) (easy to measure and analyse) and a slightly more complicated function (8) were used, the latter rendering it possible to evaluate some characteristic features of the process, such as maximum achievable spatial frequency and the change of the phase modulation depth together with the change of the spatial frequency.

The first step of the method is to transform the function describing the filter from the continuous form to a binary one. For this purpose, a number of the half-tone algorithms were analysed based on literature data ([11], [13], [15], [18]–[21]). A few of them, being most promising, were chosen for further examination and they were tested taking account of the quality of the obtained results and the speed of the data processing. These results were published earlier in [12], [22]. For the sake of experiment, two methods differing in the principle of operation, and the speed and quality of the results obtained were chosen.

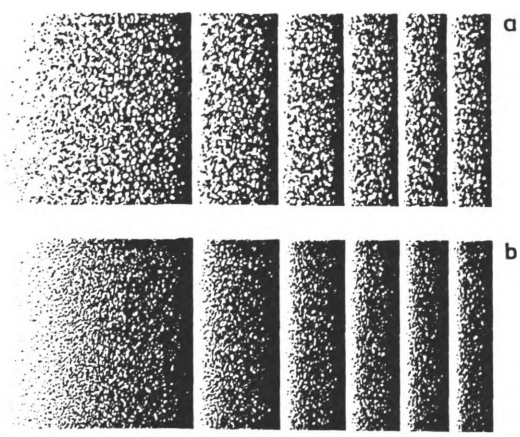

Fig. 5. Samples of half-tone image obtained by the methods of random half-toning level (a), random error diffusion (b)

The half-toning with a random threshold [13] appeared to be the quickest method, that produces a rather irregular distribution of the black and white points which often tend to cummulate giving a high granularity of the half-tone object of this kind (Fig. 5a). This method consists in comparing the values of the function $f(x, y)$ normed to range within $[0, 1]$ in each cell with a random threshold q of uniform distribution within the interval $[0, 1]$

$$B(x, y) = \begin{cases} 0 \leftrightarrow \Psi(x, y) < \text{rand}(0, 1) \\ 1 \leftrightarrow \Psi(x, y) \geqslant \text{rand}(0, 1), \end{cases} \tag{9}$$

The other half-toning method is that of random error diffusion [20], belonging to a big family of error diffusion type [11], [17]. These methods consist in assuming some value of a binary function $B(x, y)$ at a point (x, y), next the difference between this function and the original function $\Psi(x, y)$ is calculated; this difference is used to modify the values of the function $F(x, y)$ in the vicinity of the point (x, y). For the algorithm used the function $\Psi(x, y)$ was subject to the half-toning with constant threshold q equal to $q = 1/2$ in our experiment

$$B(x,y) = \begin{cases} 0 \leftrightarrow \Psi(x,y) < q \\ 1 \leftrightarrow \Psi(x,y) \geqslant q, \end{cases} \tag{10}$$

next the error of half-toning $\mathrm{Err}(x, y)$ was calculated

$$\mathrm{Err}(x,y) = \Psi(x,y) - B(x,y), \tag{11}$$

which is distributed to the closest unprocessed neighbours (Fig. 6) according to the scheme:

$$\mathrm{B}(x,y) = \begin{cases} \Psi(x+1,y) = \Psi(x+1,y) + \mathrm{rand1} \cdot \mathrm{rand2} \cdot \mathrm{Err}(x,y) \\ \Psi(x,y+1) = \Psi(x,y+1) + \mathrm{rand1}(1-\mathrm{rand2})(\mathrm{Err}(x,y), \\ \Psi(x-1,y+1) = \Psi(x-,y+1) + (1-\mathrm{rand1})\mathrm{rand3} \cdot \mathrm{Err}(x,y) \\ \Psi(x+1,y+1) = \Psi(x+1,y+1) + (1-\mathrm{rand1})(1-\mathrm{rand2})\mathrm{Err}(x,y) \end{cases} \tag{12}$$

where: rand1, rand2, rand3 are independent random variables of uniform distribution within the interval $[0, 1]$.

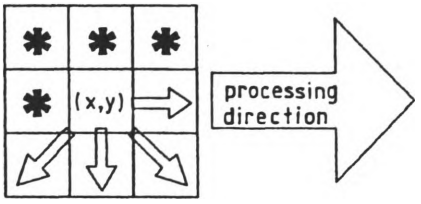

Fig. 6. Scheme of half-toning by the random error diffusion method

This method gives an irregular distribution of points well separated (Fig. 5b), *i.e.*, no local concentrations of black or white points occur, as was the case in the previous method, and also no periodic structures appear. This is, however, a much slower method than the former one in spite of the fact that it is one of the quickest methods from the error diffusion family.

Because of some limitations in the available equipment, in our experiment a function describing the filter phase was prepared in the form of a matrix 4480×4480 points, which in the half-toning process was transformed into another binary matrix of the same sizes. The last matrix was next printed on a transparency with the help of a high-resolution Hewlett–Packard laser jet printer (HPLJ4) of 600 dpi As a result, a transparent amplitude matrix of the filter of sizes 19×19 cm was obtained.

The second step of the method was photoreduction of the matrix thus prepared, made on the material creating a real filter and its photochemical processing. In the course of photoreduction, a 20-fold reduction of the sizes was carried out which, after having photographed the matrix, gave a filter of sizes 9.5×9.5 mm. The device for photoreduction (Fig. 2d) allowed us to control precisely the spread function by shifting the objective with respect to the head carrying the holographic plate.

As the recording material the 10E75 Holotest plates of Agfa–Gevaert firm were used. The photochemical processing was carried out using the standard reagents produced by Agfa–Geavert firm and 5% solution of acetic acid as a stop bath. The developed and fixed holographic plate was subject to the bleaching process [23]–[26] in a two-component self-made bleacher [26] of the following recipe: component A – potassium dichromate, sulfuric acid, component B – potassium chloride, copper sulfate, sulfuric acid. The bleacher prepared is optimal for the recording material used and allows us to achieve the theoretical efficiency $\eta \geqslant 70\%$ for bleached amplitude holograms [26]. The bleaching process was carried out until the whole silver was replaced by the due transparent salts and lasted about 10–20 min.

3.1. Course of experiment

During experiment a series of filters were made in the form of saw-tooth diffraction gratings (1) of different spatial frequencies, for different magnitudes of the spread function, using both half-toning algorithms. Next, the spread function was chosen for which a series of saw-tooth diffraction gratings were produced in order to make the measurements. Also, a series of filters of changeable spatial frequencies (7) were produced in order to observe the phenomenon of changing the modulation depth and to find the limiting frequency.

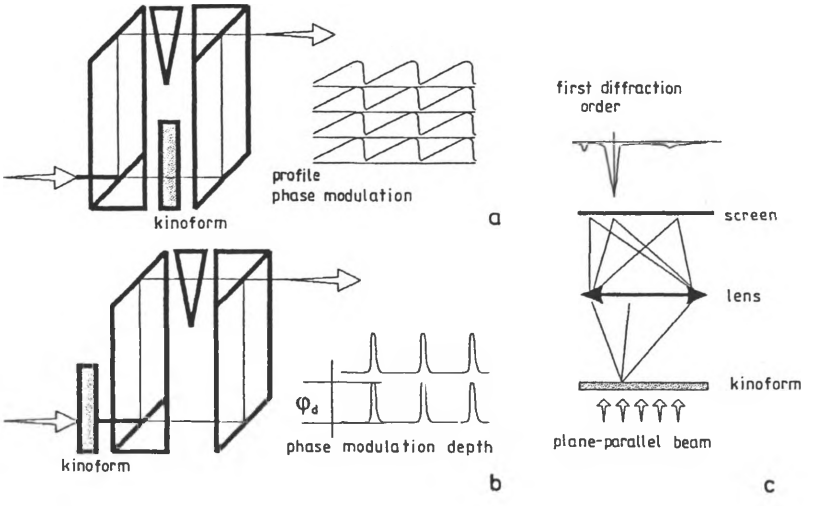

Fig. 7. Scheme of the methods of kinoform filter measurements: **a** – Mach–Zehnder interferometry, **b** – Mach–Zehnder interferometry with shearing, **c** – direct observation of diffraction at the filter

The measurements of the intermediate process, *i.e.*, the filter matrix were made. For this purpose, the objective–cassette system was replaced by CCD camera, the spread function was introduced by defocusing the camera objective (image) and the image was recorded in the computer memory. The analysis of this image allowed us to control the quality of the matrix while the whole stage of photochemical processing was avoided.

After producing the kinoform filters they were subject to examinations in the Mach–Zehnder interferometer (Fig. 7a). The measurements were made in the fringe field which gave the phase filter profile. Next, the interferometer in the Mach–Zehnder shearing system (Fig. 7b) was used, which enabled the immediate measurement of the phase modulation depth of the filter to be done. The direct observation of the diffraction at the filter was carried out (Fig. 7c).

4. Analysis and interpretation of the results

4.1. Computer simulation of the precess

The simulation done using the Matlab® ver. 4.0 program of the Simulink™ firm was applied to the second stage of the process consisting in copying the binary matrix of the filter and taking account of the spread function. For this purpose, the one-dimensional model of the filter generated by the half-toning methods was used. Also, the influence of the change in the magnitudes characterizing the filter (modulation depths, profile deformation, and so on) on the quality achieved and diffraction efficiency was examined. In this case, the function describing an ideal filter (subsec. 2.1) was applied. A series of models of saw-tooth filter of different spatial frequency ν_x

$$A(x) = A_r(x)\exp(2\pi i(\nu_x x - [\nu_x x])) \tag{13}$$

were subject to analysis together with a series of filter models of changing spatial frequencies

$$A(x) = A_r(x)\exp(2\pi i((\nu_x x)^2 - [\nu_x x]^2)). \tag{14}$$

The filter models were treated as the models of "bulk" type for which the effects of spatial frequency restrictions were negligible. In the simulation process, the filter models contained 10000–100000 single teeth depending on the spatial frequency of the given filter. This corresponds to real sizes of the generated kinoform elements. In order to obtain readable plots only some fragments of the profile of particular filters were presented.

The spreading process was simulated by a convolution of the binary filter matrix with the Gaussian function [27]

$$f(x) = \frac{1}{\sigma\sqrt{2\pi}}\exp\left(-\frac{x^2}{2\sigma^2}\right). \tag{15}$$

For the sake of convenience the Gaussian function was presented in the form

$$g(x) = \exp\left(-\frac{x^2}{\sigma^2}\right) \tag{16}$$

where the norming factor was omitted. The argument x of the function $g(x)$ was restricted within the interval $x \in [-2\sigma, 2\sigma]$, which is a sufficiently good approximation, since the values of $g(x)$ are small for $x \in (-\infty, -2\sigma) \cup (2\sigma, \infty)$ due to the shape of this function and may be neglected. The values of parameter σ define the width of the spread function so that its change allows us to simulate the spreading of different magnitude.

After having performed the calculations by using such an approximate spread function the results should be normed with a weight which was omitted when passing from the form (15) to that of (16). The weight was calculated as a reciprocal of the integral of the function $g(x)$

$$W = \left(\int_{-\infty}^{\infty} g(x)dx\right)^{-1} = \left(\int_{-2\sigma}^{2\sigma} g(x)dx\right)^{-1}. \tag{17}$$

During the analysis the examined function was compared with the ideal one (Subsec. 2.1) and similarly as was the case in Subsec. 2.2, the differences of profiles $D\varphi$ and the error of the intensity in the Fourier plane ΔI were taken into account and the diffraction efficiency of first order diffraction was calculated.

4.1.1. Cut-off frequency of the process

This simulation aided both investigation of the dependence of the diffraction efficiency of the element on its spatial frequency and determining the cut-off frequency of the method for fixed value of the spread function $g(x)$. In Subsec. 2.3 for

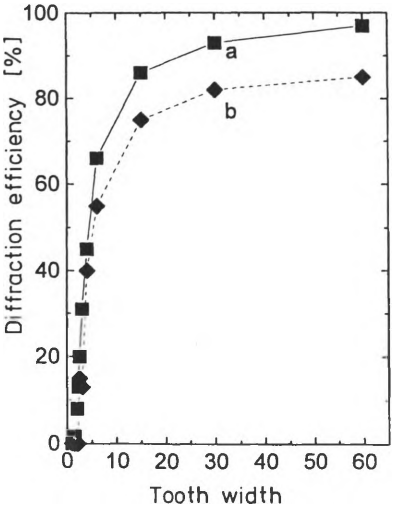

Fig. 8. Dependence of the diffraction efficiency on the spatial frequency of the saw-tooth profile for limiting case of the half-tone process (curve a) and half-toning by random half-toning method (curve b)

the limiting case (the step of half-toning being equal to zero) it has been shown that together with an increase of the spatial frequency the depth of modulation decreases while the difference between the ideal function and that subject to analysis increases.This causes a drop of filter quality and a decrease of its diffraction efficiency. The analysis was carried out for two cases: for limiting case of half-tone function (Fig. 8, curve a) and for the function half-toned by the random threshold algorithm (Fig. 8, curve b). The plots present the dependence of the diffraction efficiency η on the spatial frequency ν_x of the filter for the above two cases, the spread function being of the same width in both cases. The results obtained show high similarity while the function half-toned with the random threshold algorithm has rendered slightly worse results.

4.1.2. Influence of the half-tone algorithms on the filter quality

As mentioned above, this simulation aimed at pointing out the influence of the kind of the half-tone algorithm on the quality of the obtained filters. The analysis was performed using a saw-tooth function (1) of various spatial frequencies and the calculations were made for the random threshold algorithm and random error distribution, and next the two algorithms were compared with the limiting case of half-toning of step equal to zero (Fig. 9). The calculations were performed for various spatial frequencies of the filters obtaining similar results.

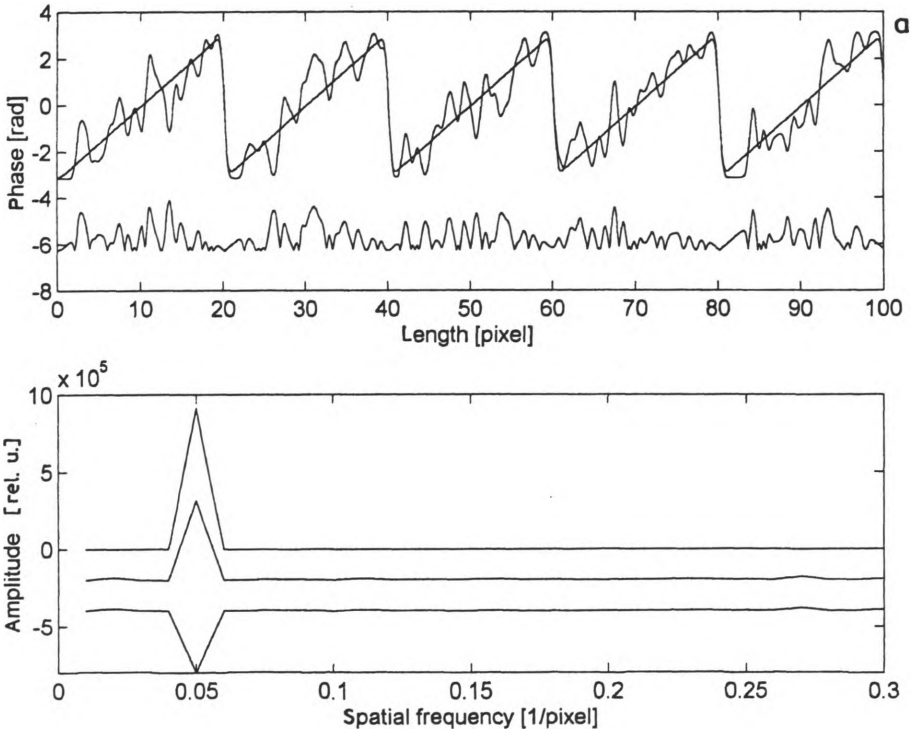

Fig. 9a

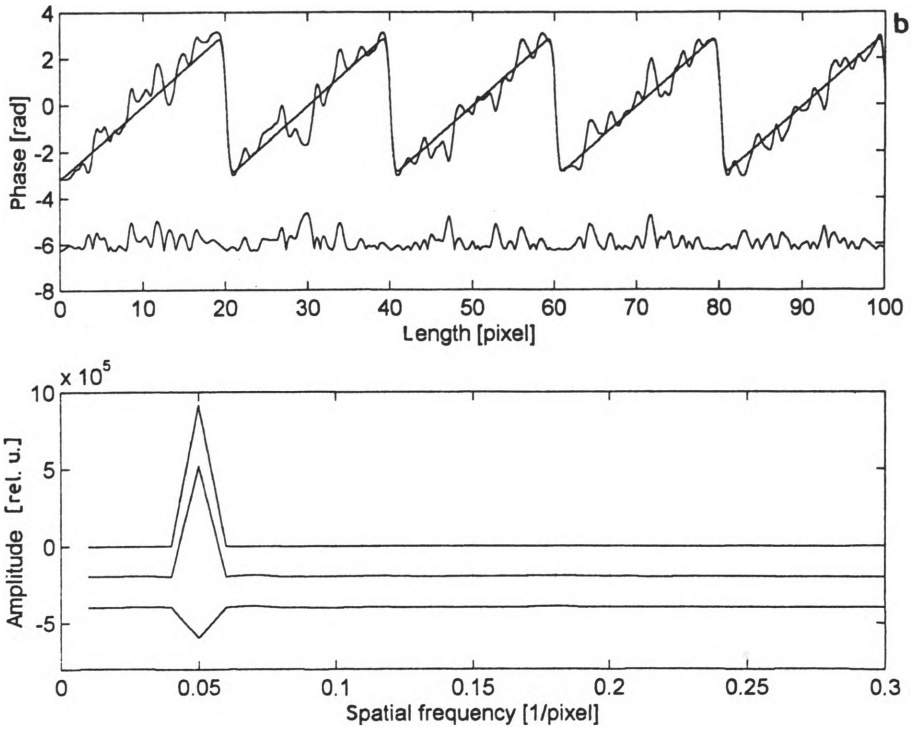

Fig. 9b

Fig. 9. Influence of the kind of half-toning algorithm on the filter profile and its intensity in the Fourier plane ΔI: **a** — random half-toning level algorithm, **b** — random error diffusion algorithm

For the random threshold algorithm the results obtained were slightly worse. In Table 1 the results obtained were compared, including: relative diffraction efficiency η_n (with respect to the limiting case of half-toning), average value of the background within the whole range of spatial frequencies (white noise) $\langle W_n \rangle$ and also the average $\langle D\varphi \rangle$ and maximal $D\varphi_{max}$ deviation of the profile obtained for the limiting case of the half-toning process.

Table 1.

Parameter/algorithm	Random error	Error diffusion
η_w	0.900	0.950
$D\varphi_{max}$	0.320	0.150
$\langle D\varphi \rangle$	0.050	0.025
$\langle W_n \rangle$	0.0090	0.0045

4.1.3. Influence of both the depth modulation and changes in transmittance on the filter quality

In the course of simulation, the changes in phase modulation depth (Fig. 10a), and in the filter transmittance (Fig. 10b) were examined, and the influence of both these effects (Fig. 11) on the appearance of other spatial frequencies in the Fourier

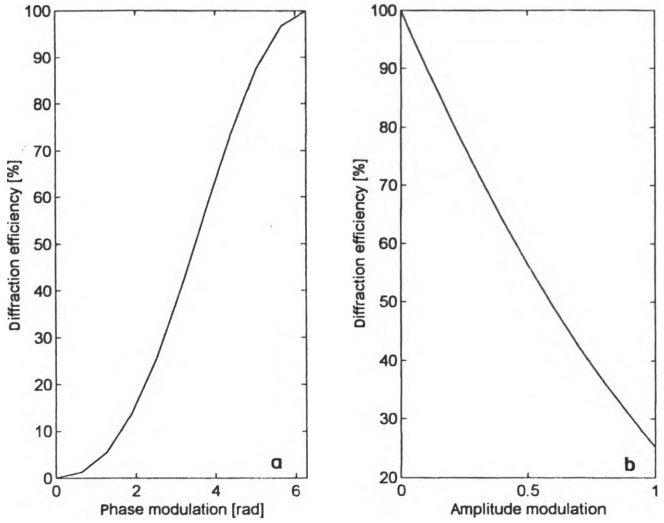

Fig. 10. Influence of the depth of: **a** — phase modulation, **b** — amplitude modulation on the filter efficiency

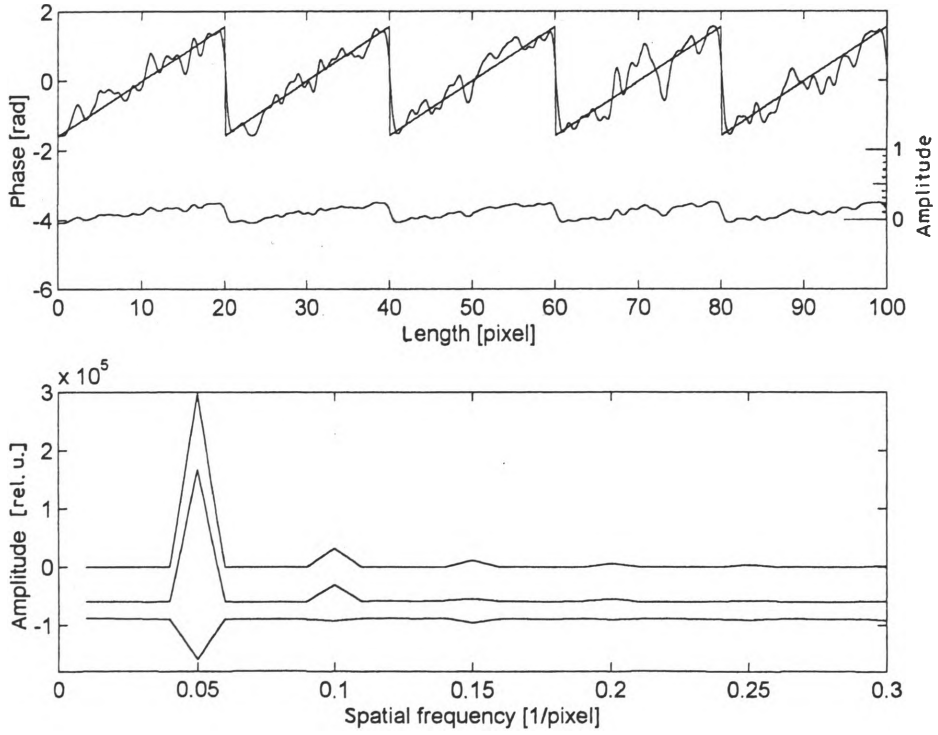

Fig. 11. Drop of the filter quality in the case of simultaneous appearance of phase modulation $\varphi_d = \pi$ and amplitude modulation $A_0 = 0.3$

spectrum (scattering in the other diffraction orders), the magnitude of the zero order diffraction and the diffraction efficiency of the filter was presented. For that purpose the intensity in the Fourier plane of the functions describing the amplitude-phase filters for suitably changing parameters $A_r(x)$ and φ_d

$$A(x) = A_r(x)\exp(i\varphi_d(x-[x])). \tag{18}$$

were compared.

The analysis was carried out for the change of modulation depth φ_d within the range $[0.3\pi, 4\pi]$ and transmittance of filter $A_r(x) = 1$, with special attention being paid to the range $[\pi, 2.5\pi]$, which occurs in the experimental realization.

When investigating the influence of the amplitude modulation of the filter it has been assumed that it is proportional to the changes of phase. This is connected with the experience that the bleaching process never causes a complete transformation of the amplitude filter into a phase one and always some residual blacking remains being proportional to the primary blacking. Its value strongly depends upon both the conditions of the process and the materials used and oscillates within the limits 0−30% [24]−[26]. When carrying out the analysis, it has been assumed that $\varphi_d = 2\pi$ and that the amplitude modulation of $A_r(x)$ takes the form

$$A_r(x) = 1 - A_0(x-[x]), \tag{19}$$

while $A_0 \in [0,1]$ and the subrange [0, 0.3] having been analysed with special care.

If both phenomena occur simultaneously as was the case in our experiment, their negative influences on the quality of the filters produced accumulate causing: the drop in diffraction efficiency in the first order of diffraction, an increase of the white noise, and a strong increase of the further diffraction orders and the zero order, as well (Fig. 11).

4.1.4. Influence of the tooth profile on the filter quality

During simulation the influence of the change of a single tooth profile on the quality of the filter has been analysed. For this purpose, the intensity in the Fourier plane of the saw-tooth diffraction grating was compared with the grating of the same spatial frequency but of changing tooth shape (Fig. 12). Three kinds of deformations with respect to ideal grating (1) were examined

$$\left.\begin{aligned} \text{a)}\ \varphi(x) &= \frac{2\pi}{\varepsilon}(x-[x]), \quad \varepsilon > x-[x] \geqslant 1 \\ \varphi(x) &= \frac{2\pi}{1-\varepsilon}(1+[x]-x), \quad \varepsilon \leqslant x-[x] \end{aligned}\right\} \frac{1}{2} \leqslant \varepsilon < 1,$$

$$\text{b)}\ \varphi(x) = 2\pi(x-[x])^{\varepsilon}, \qquad 0 < \varepsilon < 1,$$

$$\text{c)}\ \varphi(x) = 2\pi(x-[x])^{1/\varepsilon}, \qquad 0 < \varepsilon < 1. \tag{20}$$

The deformation of the first kind causes that the profile of the grating becomes more and more symmetric, which, in turn, results in light diffraction in two opposite directions (Fig. 13a) and in the limiting case $\varepsilon = 1/2$ − the same scattering at the same angle.

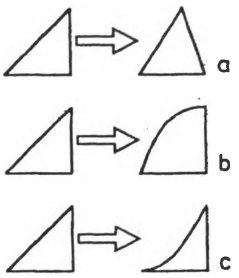

Fig. 12. Analysed kinds of tooth profile deviation from the ideal saw-tooth profile

The deformation of the second kind (Fig. 13b) and that of the third kind (Fig. 13c) determine the deviation of the tooth profile from linearity and it is responsible in practice for the nonlinear course of the following processes: the printing of the matrix, photoreduction, and, above all, the photochemical processing [23], [25].

The kind and magnitude of the deformation influence the filter efficiency (Fig. 14). For the deformation of type b and c symmetric results of the quality drop with respect to parameter ε defining the magnitude of the deviation were obtained.

4.2. Measurement of the intermediate stage – matrices

After producing the filter matrix the due measurements were performed. For this purpose the head with the cassette for the holographic plates was changed for a CCD camera. The spread function was introduced analogically by defocusing the

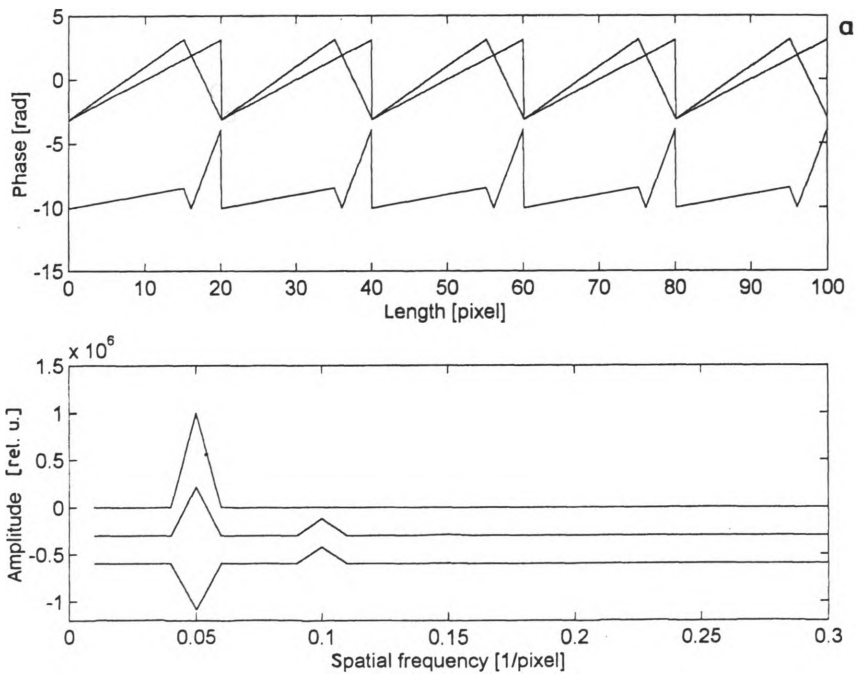

Fig. 13a

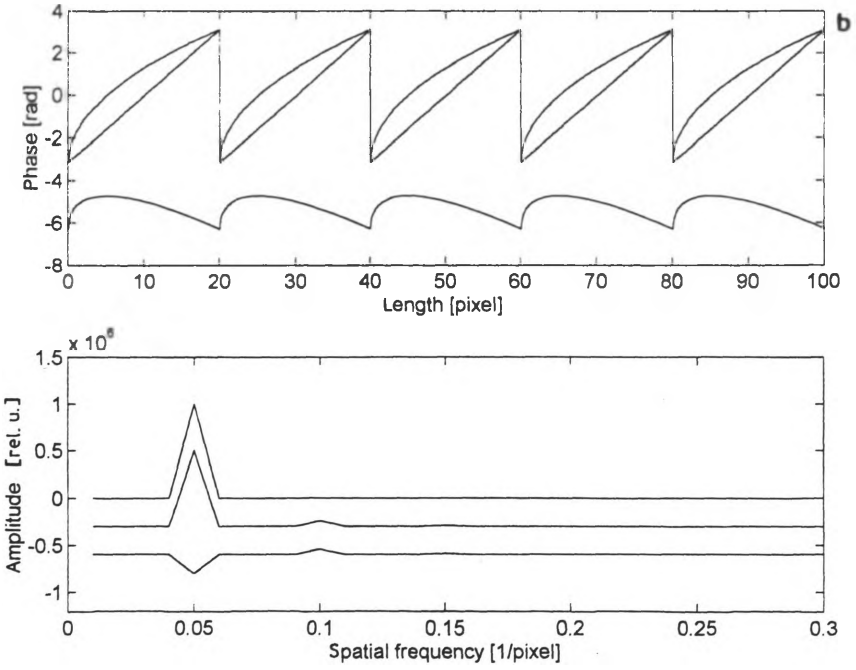

Fig. 13b

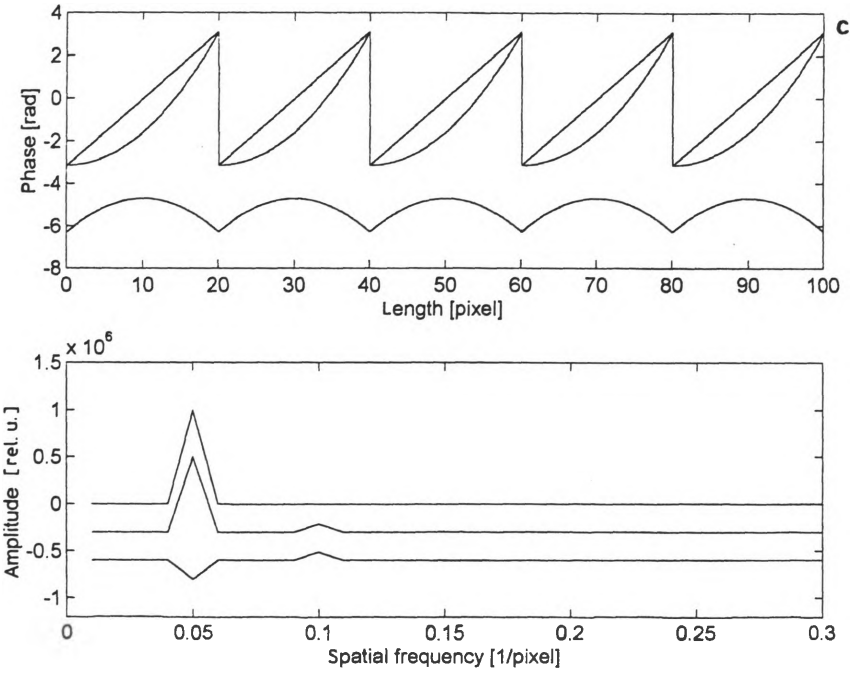

Fig. 13c

Fig. 13. Influence of the tooth profile deformation on the calculated diffraction pattern for deformations of three kinds (explanation in the text)

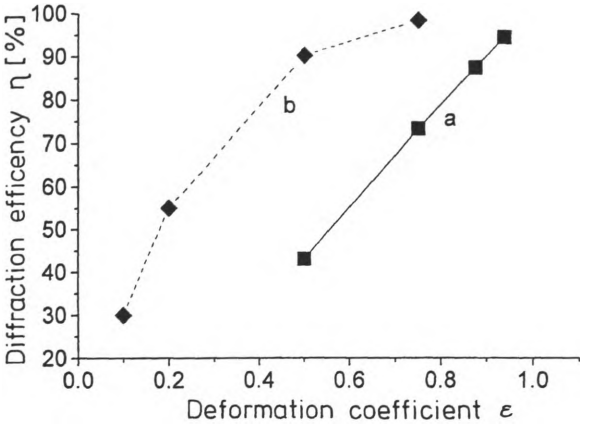

Fig. 14. Influence of the deformation measured with parameter ε on the filter diffraction efficiency: deformation type a (curve a), deformation types b and c (curve b)

objective of the camera. The image from the camera was recorded on a computer and then analysed.

The quality of the matrix production using two half-toning methods (Sec. 3) was compared. The drop of modulation depth was examined (Subsec. 4.1.1) together with the increase of the spatial frequency of the filter and it has been shown that there exists a cut-off frequency of the process. For this purpose, the measured filter profile was analysed. The linearity of the matrix performance was not checked because of nonlinear operation of the camera – framegrabber system. The filters of the teeth of changeable frequency (7) and the saw-tooth filter (1) were analysed. From the comparison of the filter profiles (Fig. 15) it follows that the random half-toning level algorithm gives slightly worse results than that of random error diffusion. The corresponding observations are compiled in Table 2.

Table 2.

Observation/algorithm	Random half-toning level	Random error diffusion
Tooth profile	High differences of the tooth profiles, distinct microstructure giving white noise	Smooth profile, almost inperceptible microstructure
Depth of modulation	Diminishing of the modulation depth with the frequency; observed cut-off frequency corresponds to the 20th tooth	Slower diminishing of the modulation depth with frequency; observed cut-off frequency corresponds to the 23rd tooth

The results of the intermediate stage are well consistent with those obtained during computer simulation.

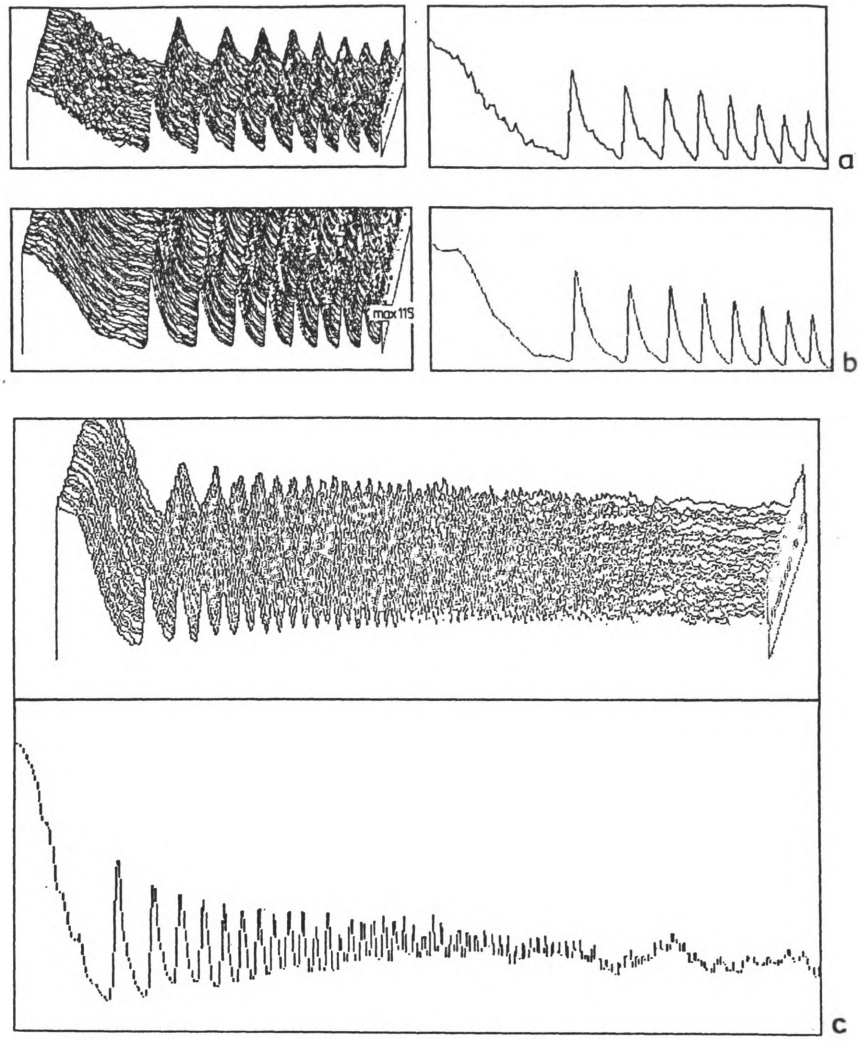

Fig. 15. Comparison of the 3D-phase surface of the matrix with diffusion and the profile cross-section for the case of saw-tooth function and half-toning algorithm: **a** — random half-toning level, **b** — random error diffusion, and **c** — function of changeable spatial frequency and random error diffusion algorithm

4.3. Measurement of the filters produced

A series of both the filters of tooth shape of changing frequency and saw-tooth filters of various spatial frequencies were produced. The parameters of the photochemical processing were chosen experimentally in order to achieve the best results — linearity of the process, depth of modulation.

The properties of the filters produced were measured and estimated using three methods (Fig. 7). The Mach—Zehnder interferometry in fringe field renders it possible to measure the profile of the phase filter and the phase modulation depth.

The Mach–Zehnder interferometry in the shearing configuration enables a simple measurement of the phase modulation depth. Direct observation of the diffraction at the element makes it possible to determine the diffraction order, to estimate the intensity of particular diffraction orders and the intensity of the background, which allows us to conclude about the diffraction efficiency of the elements produced.

4.3.1. Mach–Zehnder interferometer

In the measurement of this kind, two plane waves interfere with each other producing a fringe field if the due wavefronts are mutually inclined. After inserting a phase (or phase-amplitude) object, in one of the interferometer arms, the wave emerging from the object transports the wave disturbance introduced by the object (Fig. 7a). The interference of this wave with the plane wave is recorded on an interferogram, which thus contains the information about the phase profile of the object. Now, the comparison measurements should be made of the empty fringe field and that with the information about the object, which allows us to avoid the errors in interpretation of the fringe shape (Fig. 16 a–d) and to both determine and eliminate the errors introduced by the measuring setup.

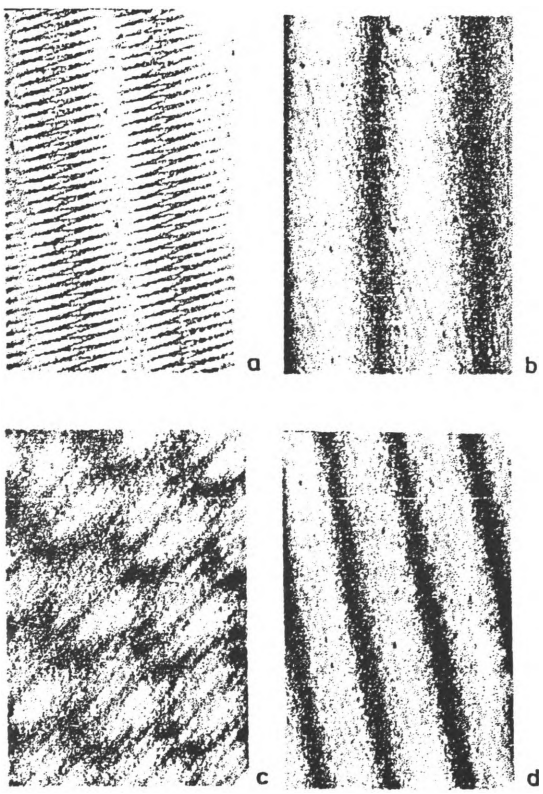

Fig. 16. Comparison of the interferogram of the field containing the object information (a, c), with an empty field (b, d)

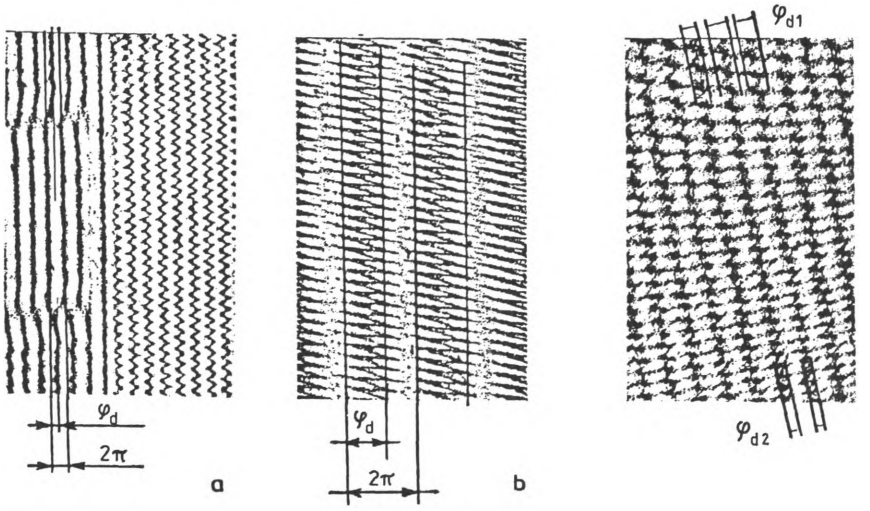

Fig. 18

Fig. 17. Kinoform phase modulation: **a** — nontransparent element measurement, **b** — measurement based on fringe profile

Fig. 18. Change of modulation depth with the change of filter spatial frequency

During performing a series of experiments in Mach–Zehnder interferometer, the majority of filter parameters were determined by direct measurement analysis and interpretation of the filter phase profile as well as by analysis of the Fourier spectrum of this profile (the latter only for saw-tooth function). The following results were obtained in experiment. Maximal phase modulation depth achieved for the material used was $\varphi_d \in [\pi, 1.3\pi]$ which corresponds to the optical path $\Delta d \in [0.5\lambda, 0.65\lambda]$, for the required kinoform value $\Delta d = \lambda$. The measurement was carried out by applying the binary filter (Fig. 17a), which was obtained from the object of transmission equal to zero, which was a metallic plate of thickness 5 mm (hence the unsharp imaged rims), and also independently by observing the filter profile (Fig. 17b). It should be mentioned that the modulation depth depends strongly on both the photochemical process and the materials used.

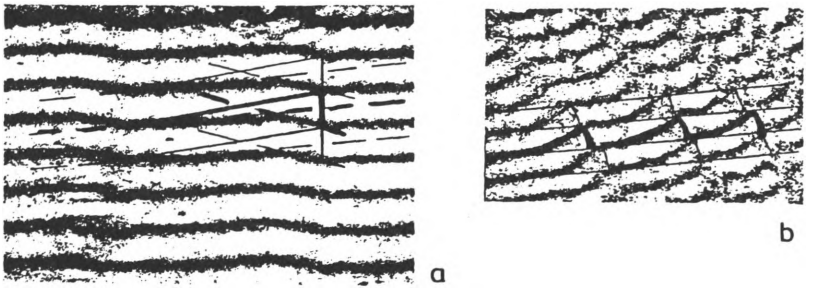

Fig. 19. Comparison of the fringe profile obtained from the measurements with that calculated theoretically: **a** — saw-tooth, **b** — changeable spatial frequency

An effect of lowering the modulation depth (Fig. 18) was observed similar to that estimated on the basis of simulation and the measurement of the intermediate stage. In contrast to this no distinct effect of appearance of the cut-off frequency was observed for which the filter structure disappears. This was caused by too narrow spread function half-width and too low spatial frequency of the filters produced. The obtained profile was well consistent with that calculated in the way of simulating both the filter of changing spatial frequency and the saw-tooth filter (Fig. 19).

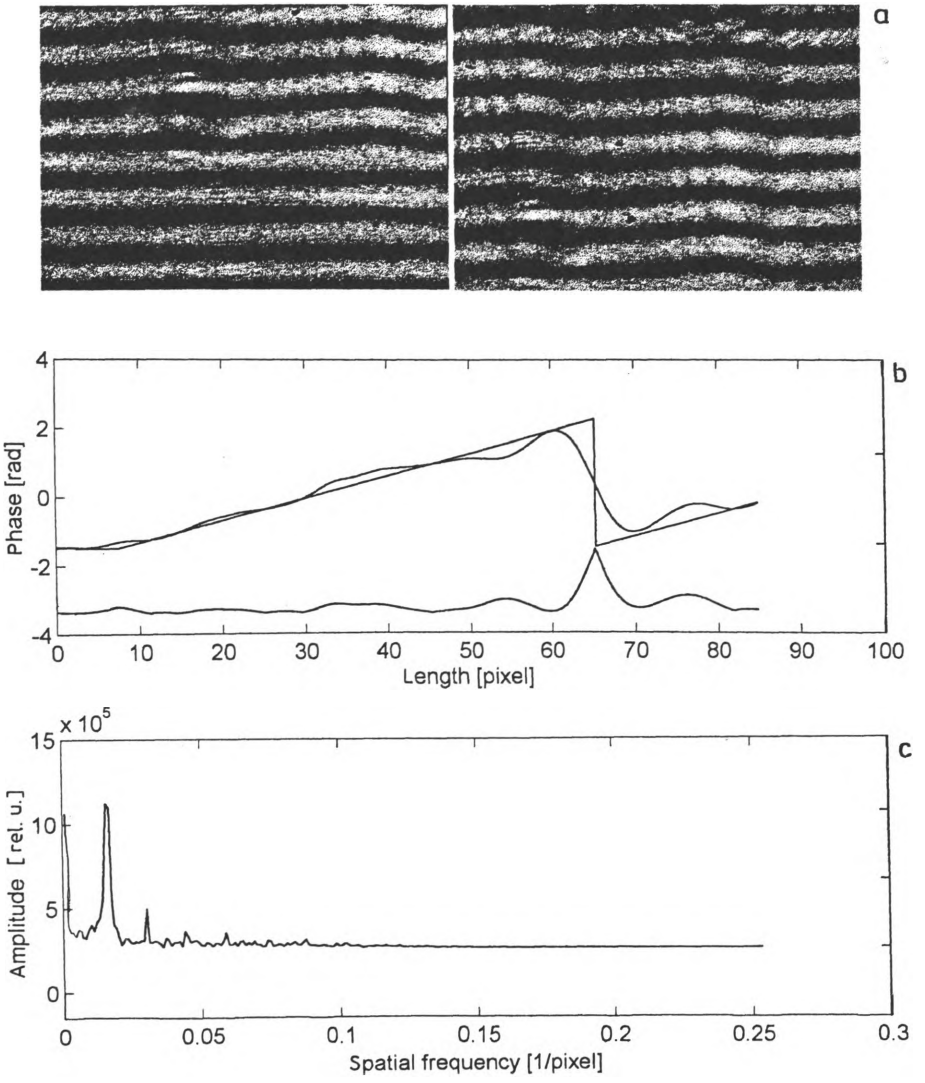

Fig. 20. Example of the saw-tooth filter: **a** — picture of profile, **b** — measured phase profile, **c** — calculated intensity in the Fourier plane

For the saw-tooth profiles of various spatial frequencies the Fourier transform (Fig. 20) and the coefficients of the diffraction efficiency η were calculated. The nearing quality of the filter production ($\eta = 65\%$) was achieved.

For the saw-tooth profile, the effect foreseen theoretically for higher spatial frequencies and consisting in deformation of the particular tooth profile in the way shown in Subsec. 4.1.4 (Fig. 12**a**) was observed. This effect appeared stronger for wider spread function (Fig. 21**b**) and weaker for narrower spread function (Fig. 21**a**).

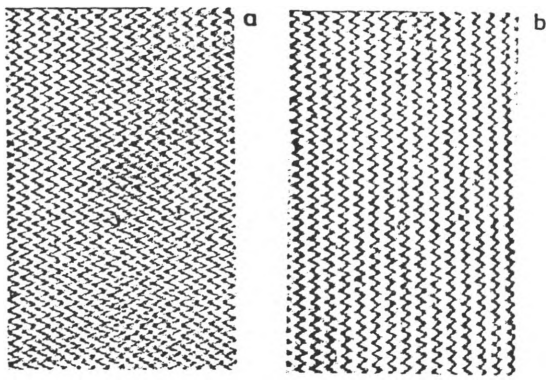

Fig. 21. Deformation of the tooth profile depending on the spread function

No significant influence of the algorithm kind on the quality of the obtained filter was observed. This can be due to the kind of experiment performed. The Mach–Zehnder interferometry belongs to the two-beam ones and consequently it gives the fringes of sinusoidal intensity distribution. Large width of these fringes (0.5π) renders it impossible to measure any deviation below 0.1π. An additional objection was the appearance of the speckles due to spatial coherence of the source. The other reason may be the fact that the photoreduction process together with the photochemical processing introduces the spread function in the way strongly reducing differences between the two analysed algorithms.

4.3.2. Mach–Zehnder interference with shearing

In this optical system the two beams carry the information about the object being slightly shifted or declined with respect to one another. As a result of their mutual interference we obtain an interference image which allows us to easily determine the phase modulation depth (Fig. 22). The measurements confirm the results obtained earlier and the modulation depth of order of $\varphi_d \in [\pi, 1.3\pi]$ was achieved.

5. Summary

5.1. Qualities and shortcomings

During the experiment a few problems appeared, with part of them being easy to eliminate. The elimination of the other part requires some modification of both the

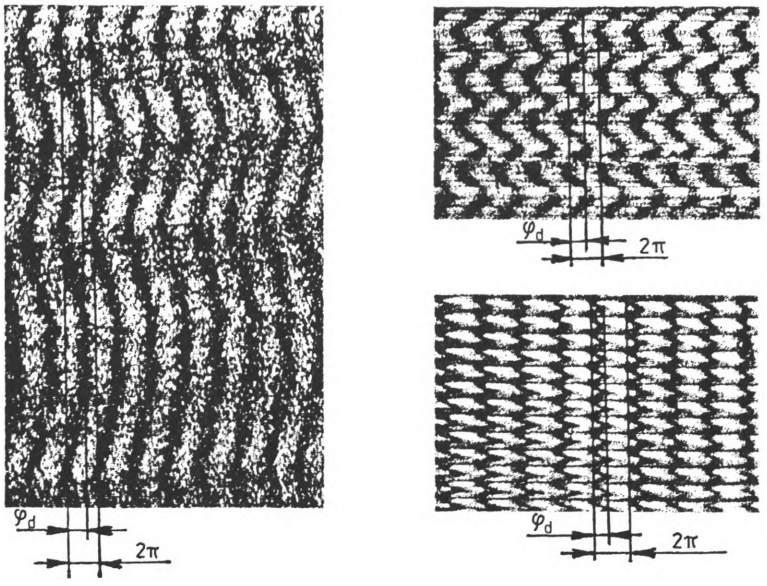

Fig. 22. Measurement of the phase modulation depth on the interferogram obtained in the Mach–Zehnder interferometer with shearing

method and the equipment as well as further examinations and performing some new direct measurements.

On the basis of observation of the appearing diffraction pattern created by the elements produced, the maximal order of diffraction, the intensity of the zero order fringe and that of continuous background were determined. The fringes were observed up to the fourth order while the third and fourth orders were very weak. The zero order fringe was of intensity comparable (though slightly less) to that of the first order fringe, the magnitude of continuous background intensity was negligible compared to the intensity of fringes. The results obtained from the observation are in good agreement with those calculated as a Fourier transform of the measured profiles of the fringes. In the future, in order to quantitatively measure the pattern a device is foreseen which is now being in the phase of designing and realization.

The stability of parameters of the printing process is difficult to achieve. In the printout there appear some structures transversal to the printing direction of period equal to the circumference of the shaft which were caused by both the construction and the working regime of the printer and could not be removed. The exchange of either toner or shaft causes a change of the printing parameters which requires each time an improvement of filter function correcting the nonlinearity effect of the printing process. Due to collecting of the electrostatic charge by the foil the latter is very susceptible to being poluted by dust which causes either some unprinted areas or overprinted areas (lack of toner, black spots) to appear. The only solution is to use the due equipment in a suitably clean room, only.

The spread function, apart from transforming the binary function to a continuous one, also broadens the elements the sharpness of which is much desired. An example of such effect is the saw-tooth function, which, after the half-toning and spreading processes, has two slopes deflecting the beam in two opposite directions. Therefore, a compromise is needed so far as the magnitude of the spread function is concerned, which, on the one hand, should improve the kinoform intensity but, on the other, causes appearance of undesirable orders of diffraction. The solution lies in increasing the printing resolution, which enables the application of the spread function of less halfwidth and, by the same means, allows us to achieve a good continuity of the elements produced, while the quantity of light diffracted in the undesirable direction is reduced. The exploitation of the professional polygraphic flood-light, working with 3600 dpi and better resolutions as well as reduction while using monochromatic light, seem to be a promising method.

Significant errors are introduced also by two-stage process of photochemical processing (development and bleaching). Above all, the process conditions are difficult to stabilize, which results in changing modulation depth and changing linearity of the profile obtained. A solution to this problem can be application of other materials (photopolymers, photoresists), and further investigation will be carried out in this direction.

The unquestionable advantages of this method are its simplicity and low cost of producing kinoforms of practically any phase profile, first of all, when manufacturing single elements to satisfy the needs of labs and teaching institutions.

5.2. Application of the method

This technique can be used to produce various phase (after bleaching) and amplitude (without bleaching) optical diffraction elements. The method seems to be ideal for production of low cost filters to be used for testing, experiment, displaying and educational purposes.

The tests in the form of saw-tooth kinoform diffraction gratings have been performed as well as kinoform spherical lenses and amplitude elements such as sinusoidal diffraction gratings, sinusoidal diffraction gratings with dislocation used to generate the wavefronts with singularites. At present, we are concentrated on production of correcting filters and those generating particular aberrations for demonstration purposes. Because of a low spatial frequency (small optical power), they should work together with a refractive lens with well corrected aberrations.

Acknowledgements — The authors are thankful to Dr. Marek Zając for his help in carrying out the experiments and interpretation of their results.

References

[1] MASAJADA J., NOWAK J., ZAJĄC M., Proc. SPIE **2169** (1993), 134.
[2] LENKOVA G. A., CHURIN E. G., Proc. SPIE **1574** (1991), 235.
[3] KORONKEVICH V. P., Avtometriya **5** (1977), 71.
[4] KORONKEVICH V. P., Optik **67** (1984), 257.

[5] ZAJĄC M., NOWAK J., Postępy Fizyki **42** (1991), 53 (in Polish).
[6] HUTLEY M. C., STEVENSEN R. E., WILSON S. J., J. Mod. Opt. **35** (1988), 265.
[7] HERZIG H. P., KAITTINEN M., EHBETS P., BLATTNER P., *Diffractive optical elements at fabrication limits*, Workshop on Diffractive Optics, Prague, August 21–23, 1995, p. 71.
[8] O'SHEA D. C., *Low cost technique for generation of kinoforms with single etching step*, Workshop on Diffractive Optics, Prague, August 21–23, 1995, p. 82.
[9] STĘPIEŃ P., *Continuous phase kinoform production by means of a high resolution binary printer*, Workshop on Diffractive Optics, Prague, August 21–23, 1995, p. 14.
[10] SLACK J. K., PARMITER P. J. M., DAINTY P., HALL T. J., IMAM H., *Fresnel elements designed by generalizing error diffusion*, Workshop on Diffractive Optics, Prague, August 21–23, 1995, p. 30.
[11] WEISSBACH S., WYROWSKI F., Appl. Opt. **31** (1992), 2518.
[12] KACZURBA M., *Metoda kodowania ciągłego rozkładu transmitancji z zastosowaniem wysokorozdzielczej drukarki laserowej* Report No. 271, Institute of Physics, TU Wrocław, 1994, (in Polish).
[13] CICHOCKI T., *Binarne filtry apodyzujące w koherentnych układach obrazujących*, Master Thesis, Institute of Physics, Warsaw University, 1992, (in Polish).
[14] RYZI Z., FIALA P., *Scanning method of production of blazed relief gratings*, Workshop on Diffractive Optics, Prague, August 21–23, 1995, p. 36.
[15] GOEBEL B., *Multilayer technology for diffractive optical elements*, Workshop on Diffractive Optics, Prague, August 21–23, 1995, p. 40.
[16] POLESHCHUK A. G., Proc. SPIE **1574** (1991), 89.
[17] BRYNGDAHL O., WYROWSKI F., [In] *Progress in Optics*, Vol. XXVIII, (1990), 1.
[18] JENNISON B. K., ALLEBACH J. P., SWEENEY D. W., J. Opt. Soc. Am. A **8** (1991) 652.
[19] BRAUER R., WYROWSKI F., BRYNGDAHL O., Appl. Opt. **31** (1992), 2535.
[20] BARNARD E., J. Opt. Soc. Am. A **11** (1988), 1803.
[21] PELI E., J. Opt. Soc. Am. A **8** (1991), 625.
[22] KACZURBA M., *Kinoformowe filtry optyczne*, Master Thesis, Institute of Physics, Technical Universtity of Wrocław, 1995 (in Polish).
[23] SOMMER S., *Proces pozytywowy i negatywowy w fotografii*, [Ed.] WAF, Warszawa 1954, (in Polish).
[24] CYPRIAN T., *Fotografia, technika i technologia*, [Ed.] WNT, Warszawa 1968, (in Polish).
[25] OSTROWSKI D. [Ed.], *Informacja obrazowa*, [Ed.] WNT, Warszawa 1992, (in Polish).
[26] KIRILLOV N. I., *Vysokorezryashayushchiie fotomateriyaly dla golografii i prociessy ikh obrabotki*, [Ed.] Nauka, Moscow 1967, (in Russian).
[27] JOŹWICKI R., *Teoria odwzorowania optycznego*, [Ed.] PWN, Warszawa 1988, (in Polish).

Received February 31, 1997
in revised form April 26, 1997